Layered seawater intrusion and melt under grounded ice

Alexander A. Robel[1], Earle Wilson[2], and Helene Seroussi[3,4]

[1]School of Earth and Atmospheric Sciences, Georgia Institute of Technology, Atlanta, GA, USA
[2]Division of Geological and Planetary Sciences, California Institute of Technology, Pasadena, CA, USA
[3]Jet Propulsion Laboratory, California Institute of Technology, Pasadena, CA, USA
[4]Thayer School of Engineering, Dartmouth College, Hanover, NH, USA

Correspondence: Alexander A. Robel (robel@eas.gatech.edu)

Abstract. Increasing melt of ice sheets at their floating or vertical interface with the ocean is a major driver of marine ice sheet retreat and sea level rise. However, the extent to which warm, salty seawater may drive melting under the grounded portions of ice sheets is still not well understood. Previous work has explored the possibility that dense seawater intrudes beneath relatively light subglacial freshwater discharge, similar to the "salt wedge" observed in many estuarine systems. In this study, we develop a generalized theory of layered seawater intrusion under grounded ice, including where subglacial hydrology occurs as a macroporous water sheet over impermeable beds or as microporous Darcy flow through permeable till. Using predictions from this theory, we show that seawater intrusion over hard beds may feasibly occur up to tens of kilometers upstream of a glacier terminus or grounding line. On the other hand, seawater is unlikely to intrude more than tens of meters through subglacial till. High-resolution simulations using the Ice-Sheet and Sea-Level System Model (ISSM) show that even just a few hundred meters of basal melt caused by seawater intrusion upstream of marine ice sheet grounding lines can cause projections of marine ice sheet volume loss to be 10-50% higher or 100% higher for kilometers of intrusion-induced basal melt. These results suggest that further observational, experimental and numerical investigations are needed to determine whether the conditions under which extensive seawater intrusion occurs and whether it will indeed drive rapid marine ice sheet retreat and sea level rise in the future.

1 Introduction

Where ice sheets come into contact with warm and salty ocean water, ice is lost through melting and dissolution. Increasing ocean-induced ice sheet melt can lead to glacier retreat and upstream glacier thinning, and ultimately contribute significantly to global mean sea level rise (Straneo and Heimbach, 2013; Shepherd et al., 2018). The grounding line (the location where glacier ice loses contact with the bed) has traditionally been considered a hydraulic barrier to the intrusion of seawater beneath grounded ice, due to the horizontal hydropotential gradient imposed by the increasing weight of a glacier that thickens upstream. Previous studies have hypothesized that seawater intrusion may only be possible when transient tidal variations in the hydrostatic pressure of seawater at the grounding line may either overcome this hydraulic barrier (Walker et al., 2013) or cause it to migrate upstream from the grounding line (Sayag and Worster, 2013). In such models, the compositional difference of seawater and subglacial discharge is not considered, leaving the horizontal variation in overburden pressure as the primary

25 control on the subglacial intrusion of seawater. However, the interface between freshwater discharge and seawater can have vertical structure where dense seawater intrudes horizontally under the lighter freshwater forming a "salt wedge", as has been observed in estuaries (Geyer and Ralston, 2011), enclosed wastewater outfalls (Adams et al., 1994), and coastal karst channels (Dermissis, 1993).

Wilson et al. (2020) first showed in theory and experiments that layered seawater intrusion is possible in laterally-confined
30 subglacial channels (i.e. Rothlisberger or Nye channels), and may extend several kilometers upstream of glacier termini under realistic conditions. A diverse range of observations have also indicated the possibility for seawater intrusion upstream of grounding lines, including: the absence of a transition in bed reflectivity across the grounding line at Whillans and Kamb ice streams (MacGregor et al., 2011), a large subglacial channel crossing the grounding line of Whillans ice stream imaged with active-source seismic methods (Horgan et al., 2013), and elevated subglacial melt upstream of the grounding line measured by
35 satellite-based interferometric synthetic aperture radar at Thwaites Glacier (Milillo et al., 2019). Such observations provide, at best, plausible arguments for the presence of seawater upstream of the grounding line, but provide few constraints on the composition, temperature, and vertical structure of these potential intrusions.

Understanding the extent of possible seawater intrusion is also directly relevant to projections of mass loss of marine ice sheets, which are highly sensitive to the intensity of ocean melt occurring near the grounding line (Arthern and Williams,
40 2017; Reese et al., 2018; Goldberg et al., 2019) and the manner in which ocean melt is applied at the grounding line in models (Seroussi and Morlighem, 2018). Ice sheet models which unintentionally include ocean melt kilometers upstream of the grounding line (due to numerical inaccuracies) simulate up to two times more Antarctic ice sheet mass loss in response to climate change over next century (Seroussi et al., 2019). Thus, investigating the possibility that seawater intrusion may drive melt under grounded ice is of first-order importance to the problem of accurately simulating the response of marine ice sheets
45 to climate change.

In this study, we generalize the channelized intrusion theory of Wilson et al. (2020) to a broader range of subglacial hydrology types which encompass most glacier grounding lines and termini (section 2). This generalized theory predicts that for the wide range of parameters describing subglacial hydrology, seawater intrusion can either be suppressed entirely, or extend 10's of kilometers inland (section 3). In a state-of-the-art ice sheet model, we show that the transient rate of ice sheet mass loss depends
50 sensitively on the distance of warm seawater intrusion upstream of marine ice sheet grounding lines (section 4). Finally, we suggest observations which may be useful to better constrain seawater intrusion and subglacial hydrology near the ice-ocean interface, and discuss the implications for simulations of future ice sheet mass loss in response to ocean warming (sections 5 and 6).

2 Theory of seawater intrusion distance beneath grounded ice

55 The goal of this study is to consider the possibility that seawater will intrude under grounded portions of ice sheets. In this section, we consider a generalized theory for the horizontal distance over which this intrusion (illustrated in Fig. 1) occurs in the cases of hard (i.e. impermeable) and soft (i.e. permeable beds). In both cases, the intrusion distance depends sensitively on
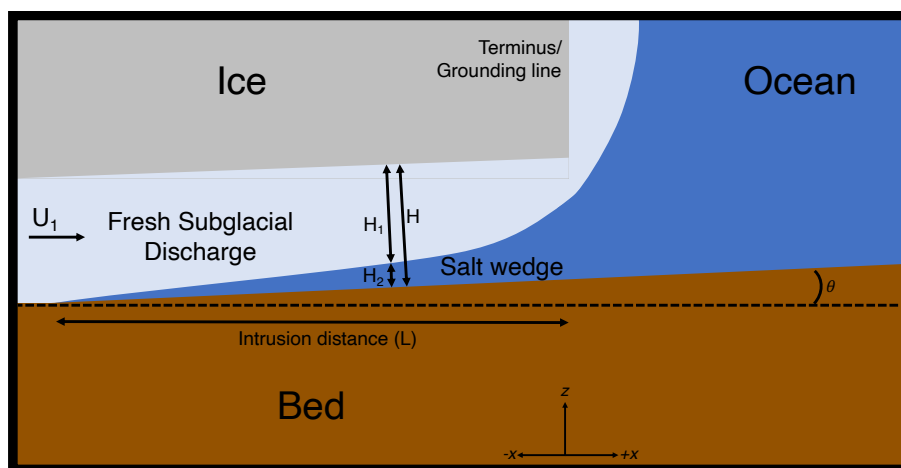
Figure 1. Illustration of salt wedge intruding under grounded ice with relevant variables labeled. Relative vertical scale exaggerated for clarity.

the characteristics of the subglacial hydrological system. In section 3, we discuss the range of predictions from this theory and the relationship to observations of subglacial hydrology.

2.1 Hard beds

On hard beds that are impermeable to vertical drainage of water, observations and theory indicate that subglacial hydrology organizes into systems that are either macroporous sheets (i.e., "inefficient" or linked-cavity drainage; Creyts and Schoof, 2009), or channelized (i.e., "efficient" drainage; Rothlisberger, 1972). If such a system is sufficiently permeable in horizontal directions, the flow can be described by the shallow water equations. If the system is less permeable in the horizontal (i.e. microporous), inertial terms become unimportant and the flow of water is better described by Darcy's law, as we discuss further in section 2.2.

Wilson et al. (2020) originally considered the dynamics of a two-layer shallow water flow for the case of a laterally and vertically confined subglacial channel on an impermeable bed, with free-flowing, fresh subglacial discharge entering a large saltwater body at rest. However, where efficient channelization does not occur, subglacial water flow likely occurs through macroporous sheets (i.e. not laterally confined) which are kept open by water pressure and the influence of large clasts protruding from the bed (Creyts and Schoof, 2009; Hewitt, 2011). We generalize the seawater intrusion theory of Wilson et al. (2020) by considering two-layer macroporous water flow through a vertically confined subglacial sheet over an impermeable bed (illustrated in Fig. 1). We will show later that the channelized system of Wilson et al. (2020) is a special intermediate case of the generalized theory derived in this study.

75   We consider a vertically confined, two-layer (fresh and saline) shallow water system, where the grounding line or terminus

is located at $X = 0$ and the layers are confined under ice where $X < 0$ (Fig. 1). Mass conservation in both layers is given by

$$\frac{\partial H_1}{\partial t} + \frac{\partial Q_1}{\partial X} = 0 \tag{1}$$

$$\frac{\partial H_2}{\partial t} + \frac{\partial Q_2}{\partial X} = 0 \tag{2}$$

where H_1 is the freshwater layer thickness, H_2 is the seawater layer thickness, $H = H_1 + H_2$ is the thickness of the sheet (i.e.

80   the confined thickness between the bed and ice), and $Q_1 = H_1 U_1$ and $Q_2 = H_2 U_2$ are the area fluxes of water of each layer,

with fluid velocities U_1 and U_2.

In the two-layer macroporous system, flow may be influenced by the relative buoyancy of the two layers, external barotropic

pressure gradients, drag from overlying ice and underlying bed, drag at the interface of the two layers, and drag from the

embedded obstacles (i.e., clasts).The momentum balance for both layers is then

85   $$\frac{\partial U_1}{\partial t} + U_1 \frac{\partial U_1}{\partial X} + \frac{1}{\rho} \frac{\partial P}{\partial X} + C_i \frac{|U_1 - U_2|(U_1 - U_2)}{H_1} + C_d U_1^2 \left(\frac{1}{H_1} + \frac{2\phi}{\pi d(1-\phi)} \right) = 0 \tag{3}$$

$$\frac{\partial U_2}{\partial t} + U_2 \frac{\partial U_2}{\partial X} + \frac{1}{\rho} \frac{\partial P}{\partial X} - C_i \frac{|U_1 - U_2|(U_1 - U_2)}{H_2} + C_d U_2^2 \left(\frac{1}{H_2} + \frac{2\phi}{\pi d(1-\phi)} \right) + g' \left(\frac{\partial H_2}{\partial x} + \tan\theta \right) = 0 \tag{4}$$

where X is the distance from the grounding line (with $X < 0$ upstream of the grounding line), t is time, $\frac{\partial P}{\partial X}$ is the along-flow

barotropic pressure gradient, C_d is the drag coefficient for flow past ice or clasts, C_i is the drag coefficient for flow at the layer

interface, ϕ is the bulk porosity of the sheet (defined as the fraction of the water sheet area occupied by obstacles), d is the

90   mean obstacle diameter, $g' = g\Delta\rho/\rho_0$ is the reduced gravity for density difference $\Delta\rho$ between the two layers, and $\tan\theta$ is the

bed slope. The main difference between this two-layer flow and that described in Wilson et al. (2020) is that the final term in

equations 3 and 4 is given by the bulk drag due to flow through a field of obstacles (Rominger and Nepf, 2011), instead of drag

due to friction at side walls. We assume in this model that the drag coefficient C_d is the same for the ice and obstacles within

the macroporous water sheet. Though this is a simplifying assumption, the uncertainty on C_d is sufficiently large itself, that it

95   encompasses the likely difference in drag properties between subglacial ice surfaces and clasts. Where freshwater discharge

is sufficiently slow, the flow of water may be considered subcritical (i.e., Froude Number, $Fr < 1$), and mixing between the

two layers is negligible (which would otherwise enter as additional terms in the above equations). Throughout this study, we

will only consider this case of subcritical flow, which is appropriate for sufficiently slow confined and unconfined estuarine

and subglacial flows, as shown in experiments (Wilson et al., 2020), and observations of weakly-forced salt wedge estuaries

100   (Ralston et al., 2010).

As can be seen in equations 3 and 4, the externally-imposed barotropic pressure gradient ($\frac{\partial P}{\partial X}$, which is known as the

subglacial hydropotential gradient among glaciologists), acts equally on both layers. A horizontal variation in this pressure due

to, for example, the bed slope or ice surface slope, is not capable of having a differential effect on the fresh and saline water

since the layers are vertically layered. Consequently, when the momentum equations are ultimately combined (below), the

105   pressure gradient falls out of the solution for intrusion distance. This model of subglacial seawater intrusion is focused on the

vertical interface of fresh and saline layers, to which the hydropotential gradient is irrelevant, and is fundamentally different

than previous efforts which focus on the horizontal interface between subglacial discharge and seawater without considering their compositional differences.

We proceed by non-dimensionalizing, combining equations 3 and 4, and making two initial assumptions: (1) that the layers achieve a steady state (i.e. all time derivatives are zero), and (2) that the saltwater layer is at rest ($U_2 = 0$). These initial assumptions are well-supported for the most general scenario of the steady layer state, no time-depending forcing, and a weak ocean circulation at the grounding line (though more complicated considerations are discussed further in section 5). The resulting equation (after H_2 is eliminated) for the freshwater layer thickness is

$$\left(Fr^2 - 1\right)\frac{\partial h}{\partial x} = Fr^2\left[\widetilde{C}_i(1-h)^{-1} + \widetilde{C}_d(1+\gamma h)\right] - \Theta \tag{5}$$

where $Fr = \frac{U_1}{\sqrt{g'H}}$ is the local dimensionless densimetric Froude number which changes with the local freshwater velocity, and dimensionless variables include $h = H_1/H$, $x = C_0 X/H$, $\widetilde{C}_i = C_i/C_0$, $\widetilde{C}_d = C_d/C_0$, $\gamma = 2\phi H/\pi d(1-\phi)$, and $\Theta = \tan\theta/C_0$, with C_0 being a characteristic scale for drag coefficients. The Froude number can be written in terms of a Froude number scale: $Fr = Fr_0 h^{-3/2}$ where $Fr_0 = \frac{U_{in}}{\sqrt{g'H}}$ is the Froude number of the freshwater inflow upstream where it occupies the entire water sheet ($\lim_{x\to-\infty} U_1(x) = U_{in}$).

At the grounding line or terminus ($x = 0$), the freshwater flow becomes unconfined and hence supercritical (i.e. $Fr = 1$), so we set the boundary condition

$$h(x = 0) = Fr_0^{2/3}. \tag{6}$$

The dimensionless intrusion distance, ℓ, is where the freshwater layer first occupies the entire subglacial water layer thickness ($h(x = \ell) = 1$), which is also where the saline layer no longer occupies any of the subglacial water layer. In appendix A, we describe how equation 5 can be numerically integrated from $x = 0$, until $h(x = \ell) = 1$, in order to find the intrusion distance, ℓ. We can also derive analytical approximations for ℓ in two limiting cases to describe how the intrusion distance depends on certain parameters describing the subglacial hydrology.

We make three simplifying assumptions to derive analytical approximations for the intrusion distance. First, we only consider flat beds ($\Theta = 0$), though we will numerically explore how sloped beds modify the intrusion distance in section 3.3. Second, we assume that interfacial drag is negligible ($C_i = 0$), as most estimates of interfacial drag between saline and fresh water layers are $O(10^{-4})$ (MacCready and Geyer, 2010; Geyer and Ralston, 2011), whereas even limiting cases of drag on relatively smooth ice walls are of order 10^{-3}, and drag is greater yet for realistic subglacial surfaces. Third, we can assume that subglacial freshwater flow is highly subcritical ($Fr_0 << 1$), which is appropriate for places like Antarctica, where there is little injection of surface melt water to the bed and subglacial water flow velocities are low (cm/s or less). With these three assumptions, equation 5 reduces to

$$\frac{\partial h}{\partial x} = \widetilde{C}_d\left(1 - \frac{h^3}{Fr_0^2}\right)^{-1}(1+\gamma h) \tag{7}$$

where we have re-written the dimensionless parameter groups involving the local Froude number in terms of h and Fr_0. This differential equation can be exactly integrated for a solution, but the resulting expression is unwieldy and hard to interpret, so we consider two end-member cases which provide reasonable lower and upper bounds on expected seawater intrusion distance.

140   The subglacial clasts which obstruct flow in the water sheet may be spaced far apart and still provide sufficient support to
maintain a separation between the ice and bed (or water pressure may maintain this separation on its own, as in Hewitt (2011)).
In this scenario, the porosity of subglacial obstacles (ϕ) is low and so $\gamma h << 1$. Equation 7 can then be integrated exactly to
yield an approximation for the intrusion distance for an unobstructed water sheet

$$\ell_u = \frac{1}{4 C_d F r_0^2}. \tag{8}$$

145 In this end-member, the dominant drag on the intrusion of seawater into the subglacial water system is the drag of the water
against the bed and against the ice. This is also the $W >> H$ (i.e., no lateral drag) limiting case of intrusion in channels
considered by Wilson et al. (2020).

        The contrasting limiting case is when clasts which obstruct flow within the water sheet are closely-spaced and so the macro-
porosity of the water sheet is high (though not sufficiently so to produce a non-inertial Darcy flow regime, which we consider
150   separately in section 2.2). In such a case, we expect that $\gamma h >> 1$, where equation 7 is integrated to yield an approximation for
the intrusion distance for a macroporous water sheet

$$\ell_p = \frac{1}{3\gamma C_d F r_0^2}. \tag{9}$$

        Re-dimensionalizing ℓ_u and ℓ_p yields upper and lower bounds on L_h ($L_h = H\ell/C_d$), the dimensional seawater intrusion
distance on hard beds, which can be written

155   $$\frac{1}{3\gamma}\tilde{L} < L_h < \frac{1}{4}\tilde{L}. \tag{10}$$

We define an "intrusion length scale" for hard beds

$$\tilde{L} = \frac{H^2 g'}{C_d^2 U_{in}^2} \tag{11}$$

which may also be derived from equation 7 using dimensional analysis. As discussed later in section 3, we generally expect
$\gamma \lesssim 6$, meaning that the intrusion distance is likely to be a fraction of the intrusion length scale between $1/4$ and $1/18$.

160   We briefly note that for the case of water flow through a subglacial channel (described in Wilson et al., 2020), the shallow
water equations have identical structure, except that $\gamma = 2H/W$, capturing the effect of drag from channel side walls (not
obstacle drag as in this model). Observations indicate that the geometry of subglacial channels spans a range from circular
(Rothlisberger, 1972), corresponding to $\gamma = 2$ in equation 9, to flat (Nye, 1976) which would correspond to an unobstructed
water sheet (equation 8). Thus, although we have focused our discussion of the macroporous water sheet, the two limiting cases
165   of ℓ_u and ℓ_p also encompass intrusion distances expected in subglacial channels. The approach of calculating two end-member
solutions for intrusion distance then provides a general theory that we expect to apply in a wide range of settings with hard
beds, regardless of the organization of the subglacial drainage.

        In Fig. 2, we evaluate the validity of the assumptions that were made on the way to deriving these analytical approximations
for the intrusion distance (purple circles) by comparing them to numerically calculated solutions to equation 5 (black lines). For
170   large γ (heavily obstructed seawater intrusion), Fig. 2a shows that ℓ_p (Equation 9) is an excellent approximation to the intrusion
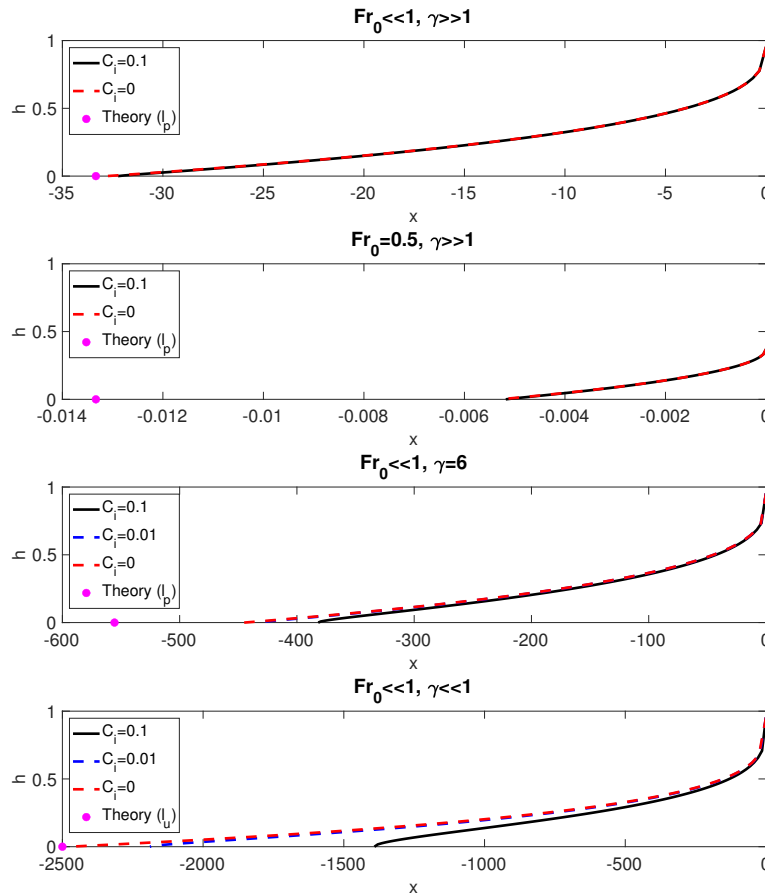
Figure 2. Comparison to analytic approximations of seawater intrusion distance, and numerical solutions of shallows water equations under various assumptions. (a) Low Froude Number ($Fr_0 << 1$) and densely obstructed macroporous water sheet flow ($\gamma >> 1$). (b) Moderate though sub-critical Froude Number ($Fr_0 = 0.5$) and densely obstructed macroporous water sheet flow ($\gamma >> 1$). (c) Low Froude Number ($Fr_0 << 1$) and moderately (though close to maximum packing fraction of spheres) obstructed macroporous water sheet flow ($\gamma = 6$). (d) Low Froude Number ($Fr_0 << 1$) and unobstructed water sheet flow ($\gamma << 1$).

distance if Fr_0 is small. Figure 2b shows that the ℓ_p approximation breaks down as Fr_0 becomes $O(1)$. At intermediate γ (Fig. 2c), ℓ_p is off by $O(1)$ as the $\gamma >> 1$ approximation becomes less appropriate. Finally, at small γ (unobstructed sheet-like flow), Fig. 2d shows that ℓ_u (Equation 8) is a good approximation if $C_i << C_d$. We note that, in general, seawater intrusion distance increases as γ and Fr_0 decrease (these dependencies are discussed in much more detail in section 3), as predicted by the analytical approximations. Ultimately, where these approximations break down, they are typically too large by factors

of $O(1)$. As we discuss later, a lack of constraints on physical parameters which enter into these analytical approximations produce uncertainties in intrusion distance range over 1-4 orders of magnitude. Thus, these approximations are good enough to provide insights into the physical controls on intrusion distance. However, where accuracy is required, numerically solving equation 5 is preferable (as we do in section 3).

2.2 Soft beds

Darcy's law is a non-inertial, creeping, incompressible simplification of the Navier-Stokes equations which describes steady-state fluid flow in microporous media. Subglacial water flow can be described by Darcy's law where there is a substantial microporous till layer beneath grounded ice. This is in contrast to the layered shallow water flow considered in the previous section where inertial and other terms are important.

The particular problem of seawater intrusion into microporous coastal aquifers where Darcy's law is a valid description of water flow has been extensively studied, due to the important implications for drinking water in coastal areas (for review see Werner et al., 2013). The canonical case of seawater intrusion into a confined aquifer considers Darcy flow where freshwater discharge flows from inland at a prescribed rate towards the ocean (identical to what is illustrated in Fig. 1). The most well-known method, due jointly to Dupuit (Dupuit, 1863) and Forchheimer (Forchheimer, 1886), assumes that hydraulic equipotential surfaces are vertical, which allows the straightforward derivation of seawater intrusion distance in a confined or unconfined porous medium. However, as Strack (1976) showed, this assumption is not strictly necessary, and a single hydraulic potential can be used to derive the horizontal extent of seawater intrusion inland in a flat, confined aquifer

$$L_s = \frac{KH}{2\alpha U_{in}} \tag{12}$$

where L_s is the dimensional seawater intrusion distance through soft permeable beds, K is the hydraulic conductivity of the microporous medium, H is the thickness of the till layer, $\alpha = 40$ is a dimensionless parameter determined by the density difference of fresh and saltwater, and U_{in} is the velocity of freshwater discharge towards the ocean (at a distance far from the ocean). This solution is widely used in the hydrology community and has been shown to predict observed and laboratory-measured seawater intrusion well (Shi et al., 2011).

On sloped beds, the geometry of the salt-freshwater interface relative to the bed slope becomes a potentially important factor in determining the intrusion distance. Where the bed deepens away from the ocean (referred to as a retrograde or reverse-slope bed in glaciology), the distance of seawater intrusion will be extended as the seawater intrusion flows downhill. For the case of a sloped confined aquifer of uniform thickness, Lu et al. (2016) extends the approach of Strack (1976), to derive an implicit equation for the horizontal extent of saltwater intrusion

$$H + L_s \tan(\theta_2) + \frac{\alpha H U_{in}}{K \tan(\theta_1)} \ln\left[1 + \frac{K \tan(\theta_1)(H - L_s \tan(\theta_2) + K \tan(\theta_1))}{\alpha U_{in}}\right], \tag{13}$$

where H is the thickness of the till layer at the grounding line and θ_1 and θ_2 are the slopes of the lower ice surface and the bed, respectively. For subglacial till layers, we don't expect the lower ice surface slope and bed slope to be significantly different over large areas (which would require the thickness of the till layer to change significantly), so we can safely assume that for

our case $\theta = \theta_1 = \theta_2$. This allows us to simplify the above implicit equation, and solve explicitly for the intrusion distance, yielding

$$L_s = -\frac{H}{\tan(\theta)} \left[1 + \frac{\alpha U_{in}}{K \tan(\theta)} \ln \left(1 - \frac{K \tan(\theta)}{\alpha U_{in}} \right) \right] \tag{14}$$

where seawater intrusion occurs if $L_s > 0$.

3 Predicted seawater intrusion distance

The theories described in the preceding section can be used to make predictions for the seawater intrusion distance expected over hard and soft beds. In this section we explore the range of seawater intrusion distances that would be predicted to occur, using the wide range of parameter values measured or indirectly inferred from observations of subglacial hydrology near grounding lines and glacier termini.

3.1 Hard beds

The intrusion length scale for hard beds (equation 11) demonstrates that there are just a few parameters that play a role in determining the horizontal seawater intrusion distance. The range of approximate analytical intrusion distances (equation 10) and those determined numerically by solving equation 5 generally are within an order of magnitude of this length scale.

The reduced gravity of the two layer system, g', is dependent on the density difference between freshwater and seawater, which will generally be near 0.27 m/s^2 if the fresh and saline layers remain distinct and unmixed, with potentially small variations due to compositional variability of either layer. As previously discussed, we assume that entrainment between layers is negligible, though we note here that g' will decrease if entrainment mixes the layers. The drag coefficient, C_d for water flow past ice or obstacles within the subglacial hydrology is typically taken to be between 10^{-3} and 10^{-2} for a range of observations typically under sea ice (Lu et al., 2011) and lab experiments for idealized walls and objects (Ezhova et al., 2018).

For realistic clast sizes, Hewitt (2011) estimated, using a mathematical model, that the natural thickness scale for a macro-porous subglacial water sheet would be 1-5 cm. Creyts and Schoof (2009) find that the thickness of steady-state subglacial water sheets is set by the size of clasts within the sheet and the water pressure maintained within the system. Antarctic tills are characterized by a wide range of particle sizes (Clarke, 2005), though tills sampled directly from Antarctic ice streams indicate the widespread presence of ploughing boulders up to 10's of cm in size. Consistent with this, MacGregor et al. (2011) estimate that a subglacial water sheet of at least 20 cm thickness exists in the grounding zones of Whillans and Kamb ice streams, with the possibility that seawater intrusion explains the persistence of high bed reflectivity across the putative grounding line (discussed further in section 5).

In the same mathematical model discussed above, Hewitt (2011) estimates water velocities in a cm-scale water sheet of 0.5-1 cm/s near the ice sheet margin. Carter and Fricker (2012) models water velocities inferred for the Siple Coast from subglacial melt production and subglacial hydropotentials also finding velocities of approximately 1 cm/s. Other studies have estimated subglacial water fluxes from basal melt (Joughin et al., 2009; Pattyn, 2010), with fluxes that are consistent with ~1 cm/s water

velocities through a ~cm thick water sheet or ~0.1 cm/s through a ~10 cm thick water sheet. Though a cm thick water sheet may
240 seem too thin to maintain stratification between layers, a highly stratified salt wedge with low mixing rates ($K_h \sim 10^{-9}$ m²/s
is the molecular diffusivity of salt in water, Kunze (2003)) will mix on a time scale of a day, by which time the stratification
will have been renewed by cm/s freshwater discharge from upstream over a km-scale seawater intrusion. For a ~10 cm water
sheet, mixing of highly-stratified layers would take months. Thus, we consider it completely plausible to maintain stratified
~cm thick water sheets if mixing between the fresh and saline layers is slow (as we have previously assumed). We also note
245 that even at more moderate levels of mixing ($K_h \sim 10^{-7}$ m²/s due to, e.g., double diffusive convection, van der Boog et al.
(2021)), water sheets ~10 cm thick are still possible to maintain.

For subglacial macroporous water sheets, $\gamma = 2\phi H / \pi d (1 - \phi)$ is dependent on the density and size of obstacles in the
macroporous subglacial water sheet. We expect that the thickness of the sheet (H) will, at most, be the typical diameter of
clastic obstacles (d), which maintain the ice-bed opening. Spherical objects of nearly similar size have a maximum packing
250 density within a two-dimensional sheet of $\phi = \pi\sqrt{3}/6 \approx 0.9$. Consequently, we expect that the maximum value of γ is likely to
be near $2/(6/\sqrt{3} - \pi) \approx 6$ (keeping in mind that nature does not necessarily arrange clasts in an optimal packing configuration).

Using this range of values for the thinnest water sheet ($H = 1$ cm), the highest drag for a smooth wall that could be supported
in such a thin water sheet ($C_d = 0.01$), and the highest water velocity ($U_{in} = 1$ cm/s), we calculate (from equation 11) a hard
bed intrusion length scale of $\tilde{L} = 2700$ meters, giving intrusion distance of 150 meters for a densely obstructed water sheet or
255 700 meters for an unobstructed water sheet (from the lower and upper bounds in equation 10, respectively). A more moderate
range of parameters ($H = 5$ cm, $C_d = 0.005$, $U_{in} = 5$ mm/s) gives intrusion distances in the range of tens of kilometers. At
the other end of the spectrum, a thick water sheet suggested by radar to exist at Siple Coast grounding zones ($H = 20$ cm
MacGregor et al., 2011), with drag coefficients appropriate for large roughness or dense clasts ($C_d = 0.01$), and low water
velocity ($U_{in} = 1$ mm/s), would suggest an intrusion length scale easily spanning the entire ice sheet interior. Maintaining
260 steady water sheet thickness in this range would require very high water pressures which may lead to turbulent flow, violating
one of the base assumptions of our theory ($Fr < 1$). We also would not expect such conditions to persist all the way into the
ice sheet interior (where subglacial water discharge and water sheet thickness are both likely to be much lower, in addition
to potential variations in bed slope). Therefore, we note this possibility, but remain skeptical that our theory would provide a
reliable prediction for seawater intrusion distance in this case.

265 Engelhardt and Kamb (1997) estimated the properties of a subglacial water sheet above till far upstream of the grounding
line of Whillans Ice Stream by injecting salt into the subglacial water system through a borehole. They inferred the water sheet
thickness and local velocity by assessing the rate at which the salt concentration decayed (assuming Poiseuille flow), resulting
in estimates of $H = 1 - 3$ mm and $U = 7$ mm/s. This is a single measurement, where the borehole is likely to have had some
influence on the local hydrology, in the interior of an ice stream where most subglacial water flow likely occurs through till
270 (see next section), and by the previous argument, is unlikely to be able to maintain stratification event for very low interfacial
mixing. However, it should be noted that if such a thin water sheet did somehow maintain two distinct layers, the extent of
seawater intrusion would not be more than tens of meters.

This extreme range in potential intrusion distance reflects the fact that subglacial hydrological parameters are uncertain over orders of magnitude and are exponentiated in equation 11, resulting in many orders of magnitude uncertainty in the intrusion

275 distance. Nonetheless, we conclude that on hard beds, seawater intrusion distances of at least 100's of meters are possible even under very conservative assumptions, and intrusion distances of 10's of kilometers are plausible. In section 4, we explore the implications of intrusion-induced basal melt over such length scales upstream of marine ice sheet grounding lines.

3.2 Soft beds

When subglacial drainage occurs by Darcy flow through confined layers of till (i.e. a "soft bed"), there is a distinct (from the

280 hard bedded case discussed above) horizontal length scale governing seawater intrusion, given by equation 12. The α parameter (analogous to g') is fairly well known for freshwater-seawater systems to be 40. H is the thickness of the confined till layer, which can range anywhere from cm to tens of meters. Similarly, the inflow rate of freshwater through till layers (U_{in}) has been estimated to be on the order of $0.1 - 1$ mm/s in ice streams where frictional heating at the ice-till interface generates high melt rates (Joughin et al., 2009). However, in regions of lower basal melt rates, we might expect inflow rates closer to $0.001 - 0.01$

285 mm/s (Pattyn, 2010).

Though H and U_{in} are uncertain over 1-4 orders of magnitude, by far the most uncertain property of subglacial till relevant to seawater intrusion is K, the hydraulic conductivity of till. The hydraulic conductivity of till gathered from formerly and currently glaciated field sites has been measured in the laboratory, and exhibits a range from 10^{-12} to 2×10^{-6} m/s (Freeze and Cherry, 1979; Cuffey and Paterson, 2010). Other methods have also been used to measure till hydraulic conductivity including:

290 in-situ measurement of borehole fluids far upstream of the grounding line at West Antarctic ice streams (Engelhardt et al., 1990) and inference from measurements of grounding line migration in different West Antarctic ice streams (Warburton et al., 2020). These other approaches to constraining till properties give a range of 10^{-9} to 10^{-4} m/s for till hydraulic conductivity.

Even though the range on the till hydraulic conductivity, thickness and inflow discharge velocities is large, we can confidently conclude that, based on the scaling given in equation equation 12, seawater intrusion into confined till layers will extend, at

295 most, meters upstream of the grounding line. For most of the range of till properties discussed above, the length scale of seawater intrusion on flat beds will be negligible. This can be compared to the range of seawater intrusion into coastal aquifers of meters to kilometers. Hydraulic conductivity of consolidated subglacial till is well known to be low compared to a typical aquifer, which is largely the reason for such small intrusion distance through flat soft beds. It is however, important to note, that previous field-based studies of till properties (particularly those reporting higher hydraulic conductivities) suggest that

300 saturation of the subglacial till layer may prevent infiltration of basal melt below the ice-till interface, leading to sheet-like flow between ice and till, more similar to the hard-bed sheet-like hydrology discussed in sections 2.1 and 3.1 (though the thickness of such a supra-till water sheet is not entirely clear). Thus, as observations from West Antarctica suggest (MacGregor et al., 2011; Horgan et al., 2013), even in places where there is substantial evidence for the existence of thick subglacial till layers, seawater intrusion may still occur through shallow water flow between ice and till.

3.3 Reverse-sloping beds

305

The intrusion of seawater under grounded ice is ultimately driven by gravity. The salt wedge is the thickest near the ocean and thins towards the glacier interior (Fig. 1), producing a pressure gradient (proportional to the salt wedge thickness gradient, $\frac{\partial h}{\partial x}$ in equation 5) that maintains the salt wedge against resistance from drag at walls, obstacles and the layer interface. On flat beds, the layer interface becomes flatter towards the interior (e.g., Fig. 2) such that eventually the drag exceeds gravitational driving, causing the termination of seawater intrusion. A bed that deepens into the glacier interior ($\theta > 0$ in equation 4 or equation 14)

310 slopes in the same direction as the salt wedge interface, and thus drives further intrusion over what would be expected on a flat bed. A sufficiently reverse-sloping bed will drive additional and potentially unbounded seawater intrusion distance (i.e., $L \rightarrow \infty$). Here we explore the criteria for "critical bed slope" beyond which seawater intrusion extends unbounded for both hard and soft beds. We will also numerically solve for the intrusion distance over a range of bed slopes and other parameter

315 values to determine generally when bed slope becomes an important driver of intrusion.
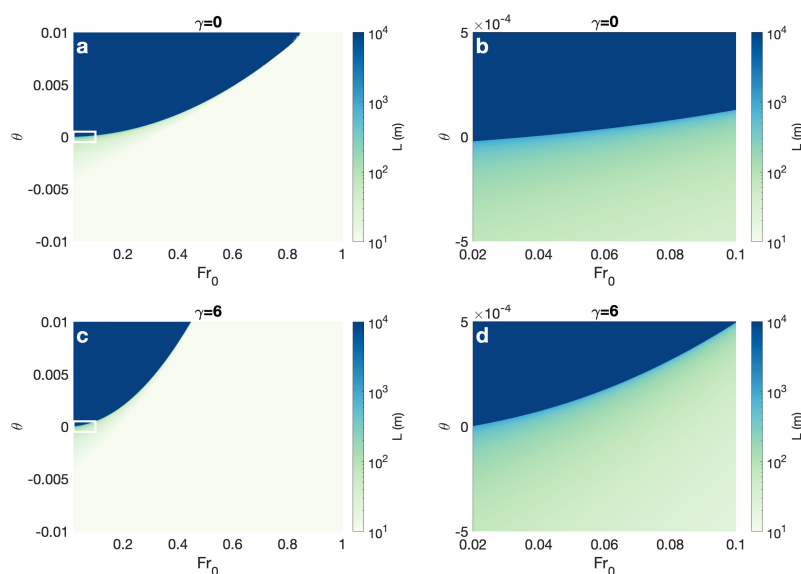

Figure 3. Seawater intrusion distance over a hard bed, calculated numerically from full model (equation 5) over a range of bed slope and Froude Number. For illustrative purposes, the bed slope ($\theta \approx \Theta C_0$) and intrusion distance ($L = \ell H/C_0$) have been shown in dimensional form for moderate parameter values ($C_0 = 0.005$ and $H = 5$ cm). (a-b) Unobstructed water sheet ($\gamma = 0$). White box in panel (a) indicates region magnified in panel (b). (c-d) Obstructed macroporous water sheet ($\gamma = 6$). White box in panel (c) indicates region magnified in panel (d). In all panels, $C_d/C_i = 10$

Following Wilson et al. (2020), we note that where the right hand side of equation 5 becomes less or equal to zero, the drag terms will never be sufficient to overcome the gravitational driving of the seawater intrusion, implying a seawater layer with

constant or growing thickness (towards the glacier interior). This implies a "critical bed slope" criterion

$$\theta > \eta C_0 Fr_0^2 \tag{15}$$

where η is a dimensionless number that is the minimum of the function $\widetilde{C}_i(1-h)^{-1} + \widetilde{C}_d(1+\gamma h)$ and C_0 is the drag coefficient scale (which is set by the obstacle/wall drag, C_d). Analytical approximation of η generally yields unwieldy expressions in terms of $\widetilde{C}_i$, $\widetilde{C}_d$ and γ. However, we can make two general observations about the scales of η before turning to numerical solution. For an unobstructed water sheet ($\gamma << 1$), η is generally $O(1)$. For a macroporous water sheet ($\gamma \sim O(1)$), η is generally $O(\gamma)$. Thus, for most realistic configurations of the subglacial water sheet ($\gamma \lesssim 6$), we expect the critical bed slope to be $O(C_0 Fr_0^2)$.

To show how bed slope affects seawater intrusion distance generally, we numerically solve equation 5, and in Fig. 3 plot the seawater intrusion distance (L) over a wide range of bed slopes and Froude numbers. What we see largely reflects the inequality in equation 15. For realistically low flow rates of subglacial discharge ($Fr_0 \sim O(0.1)$) and drag coefficients ($C_0 \sim 5 \times 10^{-3}$), seawater intrusion becomes unbounded when bed slope is steeper than $1 - 5 \times 10^{-4}$. We generally see that, for subcritical water flow ($Fr_0 < 1$) over reverse bed slopes, the critical bed slope is $O(10^{-2})$ or flatter. These bed slopes are well within the range of bed slopes found at many grounding lines at glacier termini in Greenland and Antarctica (Ross et al., 2012; Morlighem et al., 2017, 2020).
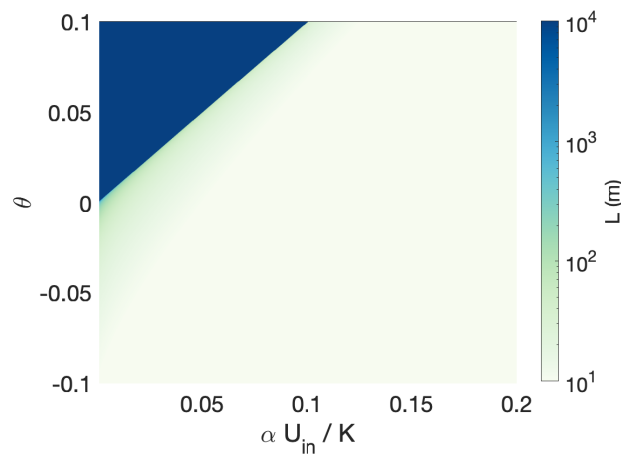

Figure 4. Seawater intrusion distance through a soft bed, calculated numerically from equation 14 over a range of bed slope and $\alpha U_{in}/K$ (a dimensionless parameter indicating the relative strength of freshwater discharge to hydraulic conductivity).

For a sloped subglacial porous aquifer, there is a similar limit in which the intrusion length becomes unbounded. This occurs when the slope of the seawater intrusion interface is less than the bed slope, thus meaning that they will never make contact (unless the bed slope or freshwater inflow changes). This occurs when the logarithm in equation 14 becomes unbounded, which is the case for

$$\theta > \frac{\alpha U_{in}}{K} \tag{16}$$

assuming $\theta \approx \tan(\theta)$. $\frac{\alpha U_{in}}{K}$ is a dimensionless parameter that quantifies the relative importance of freshwater discharge and hydraulic conductivity of the till, which together determine the "resistivity" of the till to seawater intrusion. When this parameter is large, seawater will have a difficult time intruding into the till either due to large freshwater discharge pushing back, and/or low hydraulic conductivity preventing easy flow. At the upper bound of the range of observed till hydraulic conductivity: $K \in [10^{-11}, 10^{-4}]$ and the lowest feasible freshwater flow rates in till from the interior of the catchment ($U_{in} \sim 10^{-6}$), this "resistivity" is $O(0.1)$ and the critical bed slope is in the range of the absolute steepest reverse bed slopes in either Greenland or Antarctica. Indeed, calculating seawater intrusion distance from equation 14 for a wide range of θ shows that while there are some circumstances under which seawater intrusion into till aquifers might be non-negligible (i.e. greater than meters), such conditions are seemingly rarely attained. However, it is important to emphasize that if the hydraulic conductivity of till was observed to be any higher than 10^{-4} or freshwater discharge was very low (perhaps in under a slowly flowing glacier), seawater intrusion into till would become a distinctly non-negligible possibility on reverse-sloping beds.

4 Melt from seawater intrusion beneath grounded ice sheets

Where water comes into contact with ice sheets, heat and salt are exchanged across the ice-water boundary layer (Jenkins, 1991), which may lead to dissolution or melting of ice.

Observations show that there are many places where a cold, fresh layer exists between floating ice and the warm, salty seawater, though basal melt still occurs through double-diffusive convection (Kimura et al., 2015; Begeman et al., 2018).

Where there is intrusion of a warm, saline layer under fresh, cold subglacial discharge beneath grounded ice, with subcritical water flow and limited entrainment (as previously argued), we similarly expect double-diffusive convection to maintain distinct layers while driving some ice melt that is dependent on properties of the saline layer, as has been shown in experiments and direct numerical simulations of the sub-ice boundary layers (Martin and Kauffman, 1977; Turner and Veronis, 2004; Rosevear et al., 2021). To estimate the effect of such intrusion-induced basal melt of grounded ice on the evolution of marine ice sheets, we incorporate a simple parameterization of intrusion melt into the Ice Sheet and Sea Level System Model (ISSM; Larour et al., 2012). The parameterization assumes that subglacial melt rates ($\dot{m}$) decrease linearly from the grounding line upstream, reaching zero at a specified intrusion distance, L

$$\dot{m}(x) = \dot{m}_{GL}\left[1 - \frac{x}{L}\right] \tag{17}$$

where $\dot{m}_{GL}$ is the melt rate at the grounding line (either parameterized or determined via coupling to an ocean model). In this parameterization in ISSM, x is the horizontal distance to the nearest grounding line. In an ice sheet model with explicitly simulated subglacial hydrology, x could be taken as a horizontal distance along hydropotential minima. We also specify that this parameterization is only applied upstream of the grounding line, where $0 < x < L$. Figure 5 shows an illustration of this parameterized melt rate as a function of distance from the terminus or grounding line. Though this linear decrease in melt rate is clearly a simplification of the shape of the warm salt wedges shown in Fig. 2 and does not consider the potential complexities of double-diffusive convection, our goal here is to implement a simple parameterization of intrusive melt to estimate the effect

of intrusion-driven melt under grounded ice on marine ice sheet evolution in two well-studied cases. In section 5, we discuss
370   the myriad ways that the representation of intrusion-driven melt can be made more realistic in numerical models.
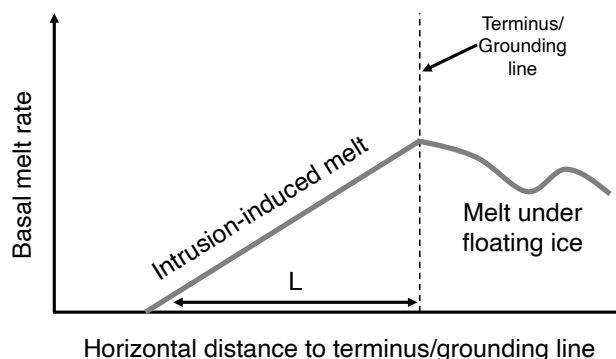

Figure 5. Illustrative schematic of a parameterization for basal melt under grounded ice caused by seawater intrusion.

    Seroussi and Morlighem (2018) show that when sub-shelf melt is applied to entire model mesh elements that are only partially floating (i.e. elements that are crossed by the grounding line), then melt intended for floating elements is "erroneously" applied to parts of elements that are not floating, just upstream of the grounding line. For typical horizontal grid resolutions (hundreds of meters to kilometers), this will lead to more rapid marine ice sheet retreat and ice loss (e.g., by up to 100%
375   compared to cases without such "errors"; Seroussi et al., 2019). Seroussi and Morlighem (2018) show how to fix this numerical issue by reducing melt rates on partially-floating model mesh elements. Though this study treats ocean melt under grounded ice as a numerical problem to be fixed, their results point to the potentially important influence of melt induced by seawater intrusion under grounded ice. Here, we have adapted the "sub-element melt 2" (SEM2) parameterization described by Seroussi and Morlighem (2018) to incorporate melt from seawater intrusion on grounded ice by calculating the "level set" horizontal
380   distance from the grounding line everywhere in the domain (x in equation 17). Intrusion distance L is specified as a model parameter and sub-shelf melt rates $\dot{m}_{GL}$ is prescribed as a constant over floating ice (though it could equally well come from a more sophisticated model for floating melt rates). In this section, we will explore the effect of different intrusion distances on transient evolution of a marine-terminating terminating glacier in two benchmark cases: the MISMIP+ idealized bed topography (Asay-Davis et al., 2016) and future evolution of Thwaites Glacier in West Antarctica (based on a well-tested
385   model configuration; Seroussi et al., 2017; Robel et al., 2019). All simulations in this section are conducted at 125 meter horizontal resolution, where errors due to the precise form of the numerical implementation of basal melt near the grounding line are negligible, as shown in Seroussi and Morlighem (2018). A convergence study shows that all results presented here using the intrusion melt parameterization are less than 3% different from equivalent simulations conducted at 250 meter horizontal resolution, confirming that these results are indeed converged in horizontal resolution.

15

4.1 ISSM Intrusion Melt: MISMIP bed topography

To demonstrate the effect of melt from seawater intrusion on ice loss from marine ice sheets, we start by using a common benchmark of marine ice sheet models, the MISMIP+ model configuration (Asay-Davis et al., 2016; Cornford et al., 2020). In this idealized configuration, a marine-terminating glacier with a buttressing ice shelf begins in a steady-state with the grounding line on a reverse-sloping bed, with no basal melt applied to the floating ice, and constant snowfall accumulation rate in space. For simplicity, in this study we consider a variant on the "Ice1r" transient experiment, in which we apply a constant melt rate on all floating ice, and then permit melt to occur with a linearly decreasing profile upstream of the grounding line according to our intrusion melt parameterization (equation 17 and Fig. 5). This constant-melt variant ensures that any dynamic feedback in response to melt forcing is due to ice sheet dynamics alone and not complicated feedbacks due to melt rate dependencies on ice sheet and bed geometry. This simplification will also allow us to straightforwardly compare the effect of adding intrusion melt over certain distances to cases without intrusion melt (in the discussion below).

In Fig. 6, we show the transient ice loss (in terms of volume above floatation, VAF) in the MISMIP+ configuration in response to various seawater intrusion distances (L in equation 17) and prescribed floating melt rates ($\dot{m}_{GL}$ in equation 17). The solid colored lines (in panel a) and colored circles (in panel b) show ice loss over 100 years with a constant melt rate on floating ice of 30 m/yr. We find a robust and significant effect of melt from seawater intrusion, with a 10-50% increase in the rate of ice volume loss for seawater intrusion over hundreds of meters, and a 50-105% increase in loss rate for intrusion over kilometers. The direct increase in ice loss from basal melt in the intrusion region generally amounts to less than 5% of the increased volume loss across experiments. Rather, it is the dynamic marine ice sheet response to melting upstream of the grounding line which is responsible for the significant increase in ice loss in the experiments with non-zero intrusion distances. Intrusion melt turns grounded ice into floating ice, which is then subject to higher melt rates and induces a greater flux of ice from upstream. The effect of 1 km of seawater intrusion is equivalent to doubling the floating melt rate without intrusion (dashed line), and the effect of 2 km of seawater intrusion is equivalent to tripling the floating melt rate without intrusion (dotted line). Though this comparison is instructive as to the large effect of intrusion-induced melt, we do emphasize that the exact sensitivity of ice loss to prescribed floating ice melt rate and intrusion distance is dependent on the particular model configuration (i.e. bed topography, extent of buttressing, initial glacier state, etc.). In the next section, we test another model configuration of interest to provide a non-idealized configuration as a point of comparison.

4.2 ISSM Intrusion Melt: Thwaites Glacier, West Antarctica

We also test effect of melt from seawater intrusion on ice loss from Thwaites Glacier (TG), a marine-terminating glacier in West Antarctica that is the focus of intense interest due to its recent acceleration and contribution to global sea level rise. The extent and intensity of submarine melting under the floating portions of TG have been studied extensively using field and remote sensing observations (Bevan et al., 2021; Wåhlin et al., 2021, e.g.,), and ocean modeling (Seroussi et al., 2017; Nakayama et al., 2019, e.g.,). In this section, we adapt the model configuration of ISSM from Seroussi et al. (2017), with a domain encompassing the TG catchment and a fine horizontal resolution. Submarine melt rates are again set to be constant at 60 m/yr which promotes
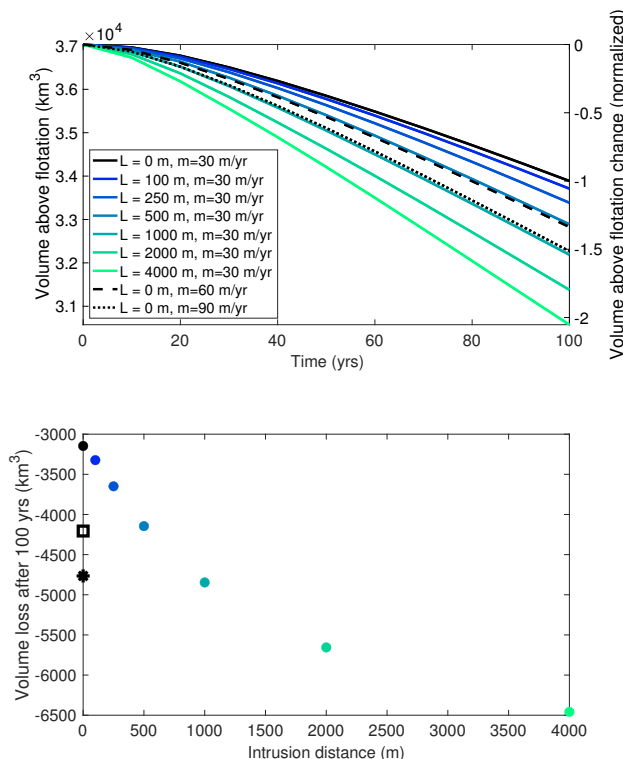
Figure 6. ISSM simulations of transient ice volume loss in the MISMIP+ configuration over 100 years with varying distances of intrusion-induced basal melt upstream of the grounding line and increased submarine melt rates with no intrusion for comparison. (a) Transient ice volume loss over 100 years. Color variation shows different prescribed intrusion distances, dashed and dotted lines show high submarine melt rates with no intrusion. (b) Total ice volume loss at the end of 100 years as a function of intrusion distance.

a rapid retreat of the TG grounding line. Surface mass balance is held constant in time and is based on regional simulations with RACMO2 averaged over the 1979-2010 time period (Lenaerts et al., 2012). The characteristics of subglacial hydrology

425 of TG have been the focus of many recent studies, with evidence for a soft bed of variable strength, and channelized hydrology near the grounding line (Schroeder et al., 2013, 2016) which sits on a steeply reverse sloping bed (Morlighem et al., 2020). These characteristics of the subglacial environment are generally favorable for the intrusion of seawater, even in particular channelized regions, which is consistent with the observations of localized high basal melt upstream of the TG grounding line by Milillo et al. (2019). However, observations of TG subglacial hydrology are still sufficiently uncertain that we simply

430 explore the potential effect of intrusion-induced melt upstream of the grounding line for the evolution of TG (similarly to the MISMIP+ case).

In Fig. 7, we show the transient ice loss over 500-year simulations in which TG retreats completely through its catchment (in all simulations). Seawater intrusion distances of hundreds of meters accelerate the onset of the most rapid retreat by decades,
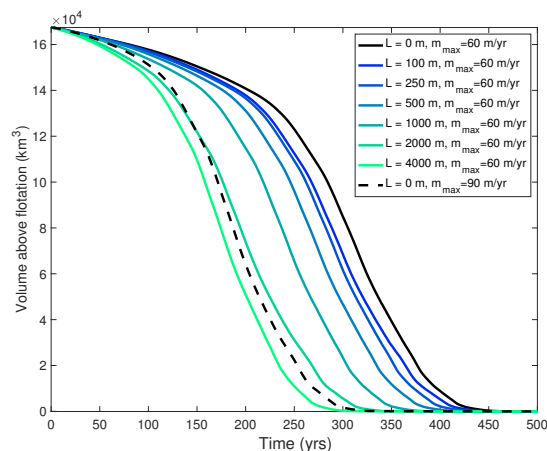
Figure 7. ISSM simulations of transient ice volume loss of Thwaites Glacier over 500 years, with varying distances of intrusion-induced basal melt upstream of the grounding line (solid colored lines) and with increased submarine melt rate with no intrusion (black dashed/dotted lines) for comparison.

and seawater intrusion over kilometers accelerates the onset of the most rapid retreat by 100-200 years. In the first 100 years of TG retreat (a common simulation period), hundreds of meters of seawater intrusion increase the rate of ice loss at TG by up to 20%, while kilometers of seawater intrusion increase the rate of ice loss by 20-100%. The effect of 2-4 km of seawater intrusion is equivalent to increasing the submarine melt rate by 50% without intrusion (dashed line). Though there are some quantitative differences between TG and MISMIP+ simulations, in the sensitivity of ice loss rate to seawater intrusion, it is generally the case that seawater intrusion of hundreds to thousands of meters (well within the range of feasibility as shown in section 3) leads to substantially more ice loss from retreating marine-terminating glaciers. These results suggest that melt from seawater intrusion could be a very important process in driving ice loss from marine ice sheets. In the next section, we discuss the implications of these results for observing the ice-ocean interface and simulating intrusion in ice sheet models.

5 Discussion

Despite the potential importance of seawater intrusion under grounded ice to the future evolution of marine ice sheets, our predictions of the horizontal extent of seawater intrusion remain uncertain over many orders of magnitude, primarily due to the lack of constraints on subglacial hydrology near the ice-ocean interface. To make better predictions of how seawater intrusion may affect future marine ice sheet evolution will require: more sophisticated numerical models of the ice-ocean interface, and more observational and experimental constraints on the properties of subglacial hydrology near the ice-ocean interface. In particular, future work can focus on answering three questions: (1) what other processes may play a role in the fluid dynamics of the freshwater-seawater interface? (2) can we definitively confirm that seawater intrusion and melt are happening under

grounded ice at some glaciers? (3) what are the properties of the subglacial hydrologic system under grounded ice near the ice-ocean interface?

5.1 Models of seawater intrusion

We have shown that the extent of potential seawater intrusion and melt under grounded ice are highly consequential for the future evolution of marine ice sheets. This is consistent with the conclusion of previous studies that have found that grounding line migration is most sensitive to basal melt at the grounding line (Arthern and Williams, 2017; Reese et al., 2018; Goldberg et al., 2019). Golledge et al. (2017) used a coarse-resolution ice sheet model in which ocean melt is applied to partially grounded elements, effectively including many kilometers of seawater intrusion in their simulations (albeit through a numerical error). Using this model, they are able to simulate collapse of the West Antarctic Ice Sheet and portions of the East Antarctic Ice Sheet during the Pliocene warm period, explaining the much higher global sea level during this period that had been a challenging target for other ice sheet models (Dutton et al., 2015). The same model (at higher resolution) has also been used to simulate the future contribution of the Antarctic Ice Sheet to sea level rise (Golledge et al., 2019), falling near the high end of the range of future model projections (Seroussi et al., 2020). Indeed, ice sheet intercomparisons have demonstrated that marine ice sheet models which apply ocean melt to elements which are partially grounded are consistently more sensitive to ocean forcing than models in which no melt is applied to these elements (increasing the Antarctic contribution to sea level rise by 50-100%; Seroussi et al., 2019). Other ice sheet dynamical mechanisms (particularly those controlling the rate of ice loss from the ice-ocean interface) have also been incorporated into models as a way of explaining the higher marine ice sheet sensitivity to climate change implied by Pliocene sea level (e.g., DeConto and Pollard, 2016). Seawater intrusion would appear to have a similar degree of support as these other sensitivity-boosting mechanisms both from fundamental theory and contemporary glaciological observations. The potential role of seawater intrusion in explaining past high sea levels and substantially increasing future projections of sea level rise suggests that this process deserves more attention through observational and modeling efforts to constrain and predict subglacial hydrology near the ice-ocean interface.

In this study, we develop reasonable approximations for the expected seawater intrusion distance over which submarine melt extends upstream of the grounding line, which can then be implemented (as shown in section 4) through an extension to grounding line melt parameterizations now common in modern ice sheet models (Seroussi et al., 2019). We also showed in theory that intrusion distance is sensitively dependent on the bed slope and subglacial hydrology. A more sophisticated treatment of seawater intrusion in an ice sheet model would dynamically calculate L at all grounding lines or termini, depending on the local bed type (hard or soft), bed slope, and state of subglacial hydrology. While the first two dependencies are relatively straightforward to accomplish in most models, most marine ice sheet models do not dynamically simulate subglacial hydrology, and those that do differ widely in the assumptions and equations used to describe evolving drainage (de Fleurian et al., 2018). The theory in this study also presumes two laminar layers that experience drag at their interface and with the surrounding solid boundaries (ice, bed, clasts or till grains). Though these assumptions allow us to develop a theory for the seawater intrusion distance, there are conditions violating these simplifications that may be relevant in some realistic cases. Where subglacial discharge is sufficiently rapid that flow can no longer be considered subcritical (i.e. $Fr > 1$) then our theory no longer

485 applies, and other considerations such as turbulent mixing and entrainment at the layer interface are likely to become important. Additionally, compositional heterogeneities and flow from the ocean could further complicate our simplified assumptions of a uniformly salty body of seawater at rest. Transient evolution of the salt wedge from tidal pumping (as in Walker et al., 2013; Sayag and Worster, 2013) or evolution of subglacial hydrology through melting by seawater may also complicate matters. Lateral heterogeneities in subglacial hydrology and other bed properties (e.g., channelization, bed slope) may lead to intrusive

490 melt at some parts of the ice-ocean interface but not others. Over time, overall terminus or grounding line retreat rate may be paced by the highest local rates of intrusion-induced melt if ice sheet flow and calving act to prevent strong curvature in the grounding line or terminus. Ultimately, the potential importance of seawater intrusion in determining the response of marine ice sheets to ocean warming necessitates high-resolution two- and three-dimensional numerical modeling of the transition between subglacial water flow (either through water sheets, channels or till) and the ocean circulation, potentially coupled to ice sheet

495 models. This study should provide the motivation for future model development in this direction.

5.2 Observations and experiments on seawater intrusion

Prior studies have found intriguing evidence of seawater intrusion in observations of grounding lines. MacGregor et al. (2011) observe no discernable change in the bed reflectivity in radar transects across the grounding lines at Whillans and Kamb ice streams, indicating a continuous water layer without a strong change in composition across this transition region (up to

500 10's of kilometers upstream). Though they ultimately attribute these observations to other factors (leaching from subglacial sediments), they do consider the possibility that seawater intrusion may explain these observations (though ultimately dismiss this possibility due to the subglacial hydropotential gradient argument, discussed in section 2.1). Horgan et al. (2013) observe a subglacial channel across the grounding line of Whillans Ice Stream (at a different location from MacGregor et al. (2011)) using active seismic methods, and argue that the weak hydraulic potential would suggest the potential for tidal pumping of seawater

505 upstream of the grounding line as in an estuary. Such an observation is fully consistent with the independent observations of MacGregor et al. (2011), and the "estuary-like" salt wedge described here and previously for channels in Wilson et al. (2020), though the theory does not require tides for seawater to intrude past the grounding line. Milillo et al. (2019) observed subglacial melt from satellite-based Interferometric Synthetic Aperture Radar kilometers upstream of the grounding line along channelized pathways. Though catchment-spanning seawater intrusion is likely ruled out by the lack of seawater observed in

510 boreholes drilled to the bed far upstream (100's of km) of the grounding line (Tulaczyk et al., 2014), there are indications of high-salinity water far upstream of the grounding line in recent electromagnetic observations (Gustafson, 2020).

Interferometry, sounding radar, and seismic methods provide complementary observations of the ice-bed interface (e.g., bed reflectivity, melt rate, acoustic impedance). More recent advances in radar technology and processing (e.g., ApRES, full-waveform inversion) and electromagnetic methods (Key and Siegfried, 2017) hold promise to better constrain the structure of

515 subglacial water system (e.g., H), pore-water properties, the salinity of subglacial water, and basal melt rates at high resolution across the grounding line. Providing better constraints on the velocity of subglacial water flow from upstream (U_{in}) in either till or subglacial water sheets would likely require either direct access through borehole drilling near the grounding line (as in Engelhardt and Kamb, 1997, but closer to the grounding line) or model-based estimates of meltwater production upstream

(Joughin et al., 2009; Pattyn, 2010; Carter and Fricker, 2012). Additionally, drag coefficients for a wider range of subglacial

520 conditions and obstacle types can be better constrained with experimental techniques, though only limited efforts have been made in this direction (Prohaska, 2017). Ultimately, targeted efforts to observe seawater intrusion in the field would provide important constraints on the theory developed in this study.

6 Conclusions

The interface of ice, ocean, and the solid Earth plays host to a complex array of processes that drive much of the changes

525 observed at marine-terminating glaciers. This study considers one such process, the intrusion of seawater under grounded ice. We extend the theory of layered seawater intrusion under grounded ice developed for channels by Wilson et al. (2020), to a generalized theory for seawater intrusion under grounded ice in a wide range of possible subglacial hydrological systems. We find that there is a wide range of seawater intrusion distances predicted by this generalized theory, which includes cases with effectively no intrusion, but also up to tens of kilometers of intrusion (and potentially even further) in macroporous water sheets

530 (or channels) over impermeable beds. Seawater intrusion is generally negligible through microporous till layers, but under the rights circumstances (steep reverse bed slopes, high hydraulic conductivity) till can support substantial intrusion, analogous to seawater intrusion in porous coastal aquifers. Seawater intrusion may also melt grounded ice, which can more than double the rate of transient ice loss from marine ice sheets under the right circumstances. This finding is in line with previous studies which have found strong sensitivity of the projected contribution of marine ice sheets to future sea level rise to the numerical

535 treatment of basal melt just upstream of grounding lines in ice sheet models (Seroussi et al., 2019).

This study demonstrates that seawater intrusion under grounded ice is theoretically possible (even expected) and has substantial implications for projections of future sea level rise from marine ice sheet retreat under climate change. To determine whether seawater intrusion actually occurs in reality, targeted observational campaigns and experiments are needed to investigate the subglacial hydrology and melt rates near grounding lines and glacier termini. Additionally, intrusion-induced melt

540 should be incorporated deliberately (rather than as a numerical artifact) in ice sheet models used for sea level projections. High resolution experimental and numerical approaches are also needed to understand the potential role of turbulence, tides and other important processes in either supporting or suppressing seawater intrusion. Though seawater intrusion has thus far been understudied as a potential driver of ice sheet changes, we hope that synthesizing theoretical and modeling approaches to intrusion will catalyze future efforts to better under this elusive process.

545 *Code availability.* All Python and MATLAB scripts used to produce the figures in this manuscript are freely available in a public GitHub repository: https://github.com/aarobel/IntrusionUnderIceSheets. The results of sections 2-3 can also be reproduced interactively in the cloud using the binderized Jupyter notebook: https://mybinder.org/v2/gh/aarobel/IntrusionUnderIceSheets/master?filepath=SeawaterIntrusionUnderIce.ipynb. The ISSM software package is publicly available for download from https://issm.jpl.nasa.gov/.

The Cryosphere
Discussions

Appendix A: Numerical solutions for seawater intrusion distance on hard beds

550   In this study, we present various analytic approximations in certain limits for the seawater intrusion distance. The seawater intrusion distance is defined as the location where $h(x) = 1$ governed by the ordinary differential equation

$$\left(Fr^2 - 1\right)\frac{\partial h}{\partial x} = Fr^2 \left[\widetilde{C}_i(1-h)^{-1} + \widetilde{C}_d(1+\gamma h)\right] - \Theta \tag{A1}$$

where $Fr = Fr_0 h^{-3/2}$ and we have a single boundary condition $h(x=0) = Fr_0^{2/3}$. This problem is an initial value problem where the unknown is the value of x at which a certain criteria is satisfied. Therefore, it is simple enough to integrate the above

555   equation numerically, starting from $x = 0$ and continuing to march towards lowers value of x until the criteria is satisfied.

However, there is one aspect of this problem which requires care in the marching scheme, namely that $Fr(x=0) = 1$ introduces a singularity in dh/dx. Though there are sophisticated ways to handle such an issue analytically, to facilitate a straightforward numerical solution, we simply set $Fr(x=0) = 1 - \sqrt{\epsilon}$ where $\epsilon = 10^{-16}$ is a machine-precision perturbation to the Froude number, and use a variable resolution marching scheme, where

560   $$dx = \epsilon + (dx_0 - \epsilon)\tanh\left[\left(\frac{dh}{dx}\right)^{-1}\right], \tag{A2}$$

where dx_0 is a larger step size (we use 0.1). This approach will ensure this method accurately captures the boundary layer near $x = 0$ where h changes rapidly and the step size needs to be quite small, while using a more computationally efficient large step size dx_0 away from the boundary layer where h is changing more slowly.

Author contributions. AAR and EW conceived the study based on EW's prior work. AAR and HS modified ISSM and AAR conducted the
565   ISSM simulations. AAR wrote the manuscript with contributions from all authors.

References

Adams, E. E., Sahoo, D., Liro, C. R., and Zhang, X.: Hydraulics of seawater purging in tunneled wastewater outfall, Journal of Hydraulic
Engineering, 120, 209–226, 1994.

Arthern, R. J. and Williams, C. R.: The sensitivity of West Antarctica to the submarine melting feedback, Geophysical Research Letters, 44,
2352–2359, 2017.

Asay-Davis, X. S., Cornford, S. L., Durand, G., Galton-Fenzi, B. K., Gladstone, R. M., Gudmundsson, G. H., Hattermann, T., Holland,
D. M., Holland, D., Holland, P. R., et al.: Experimental design for three interrelated marine ice sheet and ocean model intercomparison
projects: MISMIP v. 3 (MISMIP+), ISOMIP v. 2 (ISOMIP+) and MISOMIP v. 1 (MISOMIP1), Geoscientific Model Development, 9,
2471–2497, 2016.

Begeman, C. B., Tulaczyk, S. M., Marsh, O. J., Mikucki, J. A., Stanton, T. P., Hodson, T. O., Siegfried, M. R., Powell, R. D., Christianson,
K., and King, M. A.: Ocean stratification and low melt rates at the Ross Ice Shelf grounding zone, Journal of Geophysical Research:
Oceans, 123, 7438–7452, 2018.

Bevan, S. L., Luckman, A. J., Benn, D. I., Adusumilli, S., and Crawford, A.: Brief Communication: Thwaites Glacier cavity evolution, The
Cryosphere Discussions, pp. 1–12, 2021.

Carter, S. and Fricker, H.: The supply of subglacial meltwater to the grounding line of the Siple Coast, West Antarctica, Annals of Glaciology,
53, 267–280, 2012.

Clarke, G. K.: Subglacial processes, Annu. Rev. Earth Planet. Sci., 33, 247–276, 2005.

Cornford, S. L., Seroussi, H., Asay-Davis, X. S., Gudmundsson, G. H., Arthern, R., Borstad, C., Christmann, J., Dias dos Santos, T., Feld-
mann, J., Goldberg, D., et al.: Results of the third Marine Ice Sheet Model Intercomparison Project (MISMIP+), The Cryosphere, 14,
2283–2301, 2020.

Creyts, T. T. and Schoof, C. G.: Drainage through subglacial water sheets, Journal of Geophysical Research: Earth Surface, 114, 2009.

Cuffey, K. and Paterson, W.: The Physics of Glaciers, Pergamon, 3rd edn., 2010.

de Fleurian, B., Werder, M. A., Beyer, S., Brinkerhoff, D. J., Delaney, I., Dow, C. F., Downs, J., Gagliardini, O., Hoffman, M. J., Hooke,
R. L., et al.: SHMIP The subglacial hydrology model intercomparison Project, Journal of Glaciology, 64, 897–916, 2018.

DeConto, R. M. and Pollard, D.: Contribution of Antarctica to past and future sea-level rise, Nature, 531, 591–597, 2016.

Dermissis, V.: Seawater intrusion in submarine karst channel of rectangular cross-section, WIT Transactions on Ecology and the Environ-
ment, 2, 1993.

Dupuit, J.: Études théoriques et pratiques sur le mouvement des eaux dans les canaux découverts et à travers les terrains perméabls: avec
des considérations relatives au régime des grandes eaux, au débouché à leur donner, et à la marche des alluvions dans les rivières à fond
mobile, Dunod, 1863.

Dutton, A., Carlson, A., Long, A., Milne, G., Clark, P., DeConto, R., Horton, B., Rahmstorf, S., and Raymo, M.: Sea-level rise due to polar
ice-sheet mass loss during past warm periods, Science, 349, aaa4019, 2015.

Engelhardt, H. and Kamb, B.: Basal hydraulic system of a West Antarctic ice stream: constraints from borehole observations, Journal of
Glaciology., 43, 207–230, 1997.

Engelhardt, H., Humphrey, N., Kamb, B., and Fahnestock, M.: Physical conditions at the base of a fast moving Antarctic ice stream, Science,
248, 57–59, 1990.

Ezhova, E., Cenedese, C., and Brandt, L.: Dynamics of three-dimensional turbulent wall plumes and implications for estimates of submarine glacier melting, Journal of Physical Oceanography, 48, 1941–1950, 2018.

Forchheimer, P.: Über die Ergiebigkeit von Brunnen-Anlagen und Sickerschlitzen [On the yield of well fields and drainage trenches],
610   Zeitschrift des Architekten-und Ingenieur-Vereins zu Hannover, 32, 540–564, 1886.

Freeze, R. A. and Cherry, J. A.: Groundwater, Prentice Hall, 1979.

Geyer, W. and Ralston, D.: 2.03—The dynamics of strongly stratified estuaries, Treatise on Estuarine and Coastal Science. Amsterdam: Elsevier, pp. 37–52, 2011.

Goldberg, D., Gourmelen, N., Kimura, S., Millan, R., and Snow, K.: How accurately should we model ice shelf melt rates?, Geophysical
615   Research Letters, 46, 189–199, 2019.

Golledge, N. R., Thomas, Z. A., Levy, R. H., Gasson, E. G., Naish, T. R., McKay, R. M., Kowalewski, D. E., and Fogwill, C. J.: Antarctic climate and ice-sheet configuration during the early Pliocene interglacial at 4.23 Ma, Climate of the Past, 13, 959–975, 2017.

Golledge, N. R., Keller, E. D., Gomez, N., Naughten, K. A., Bernales, J., Trusel, L. D., and Edwards, T. L.: Global environmental consequences of twenty-first-century ice-sheet melt, Nature, 566, 65–72, 2019.

620   Gustafson, C. D.: Electromagnetic Investigations of Submarine and Subglacial Hydrogeologic Systems, Ph.D. thesis, Columbia University, Palisades, NY, 2020.

Hewitt, I.: Modelling distributed and channelized subglacial drainage: the spacing of channels, Journal of Glaciology., 57, 302–314, 2011.

Horgan, H. J., Alley, R. B., Christianson, K., Jacobel, R. W., Anandakrishnan, S., Muto, A., Beem, L. H., and Siegfried, M. R.: Estuaries beneath ice sheets, Geology, 41, 1159–1162, 2013.

625   Jenkins, A.: A one-dimensional model of ice shelf-ocean interaction, Journal of Geophysical Research: Oceans, 96, 20 671–20 677, 1991.

Joughin, I., Tulaczyk, S., Bamber, J. L., Blankenship, D., Holt, J. W., Scambos, T., and Vaughan, D. G.: Basal conditions for Pine Island and Thwaites Glaciers, West Antarctica, determined using satellite and airborne data, Journal of Glaciology, 55, 245–257, 2009.

Key, K. and Siegfried, M. R.: The feasibility of imaging subglacial hydrology beneath ice streams with ground-based electromagnetics, Journal of Glaciology, 63, 755–771, 2017.

630   Kimura, S., Nicholls, K. W., and Venables, E.: Estimation of ice shelf melt rate in the presence of a thermohaline staircase, Journal of Physical Oceanography, 45, 133–148, 2015.

Kunze, E.: A review of oceanic salt-fingering theory, Progress in Oceanography, 56, 399–417, 2003.

Larour, E., Seroussi, H., Morlighem, M., and Rignot, E.: Continental scale, high order, high spatial resolution, ice sheet modeling using the Ice Sheet System Model (ISSM), Journal of Geophysical Research: Earth Surface, 117, 2012.

635   Lenaerts, J., Van den Broeke, M., van de Berg, W. J., van Meijgaard, E., and Kuipers Munneke, P.: A new, high-resolution surface mass balance map of Antarctica (1979–2010) based on regional atmospheric climate modeling, Geophysical Research Letters, 39, 2012.

Lu, C., Xin, P., Kong, J., Li, L., and Luo, J.: Analytical solutions of seawater intrusion in sloping confined and unconfined coastal aquifers, Water Resources Research, 52, 6989–7004, 2016.

Lu, P., Li, Z., Cheng, B., and Leppäranta, M.: A parameterization of the ice-ocean drag coefficient, Journal of Geophysical Research: Oceans,
640   116, 2011.

MacCready, P. and Geyer, W. R.: Advances in estuarine physics, Annual Review of Marine Science, 2, 35–58, 2010.

MacGregor, J. A., Anandakrishnan, S., Catania, G. A., and Winebrenner, D. P.: The grounding zone of the Ross Ice Shelf, West Antarctica, from ice-penetrating radar, Journal of Glaciology, 57, 917–928, 2011.

Martin, S. and Kauffman, P.: An experimental and theoretical study of the turbulent and laminar convection generated under a horizontal ice
645   sheet floating on warm salty water, Journal of Physical Oceanography, 7, 272–283, 1977.

Milillo, P., Rignot, E., Rizzoli, P., Scheuchl, B., Mouginot, J., Bueso-Bello, J., and Prats-Iraola, P.: Heterogeneous retreat and ice melt of
      Thwaites Glacier, West Antarctica, Science advances, 5, eaau3433, 2019.

Morlighem, M., Williams, C. N., Rignot, E., An, L., Arndt, J. E., Bamber, J. L., Catania, G., Chauché, N., Dowdeswell, J. A., Dorschel, B.,
      et al.: BedMachine v3: Complete bed topography and ocean bathymetry mapping of Greenland from multibeam echo sounding combined
650   with mass conservation, Geophysical research letters, 44, 11–051, 2017.

Morlighem, M., Rignot, E., Binder, T., Blankenship, D., Drews, R., Eagles, G., Eisen, O., Ferraccioli, F., Forsberg, R., Fretwell, P., et al.:
      Deep glacial troughs and stabilizing ridges unveiled beneath the margins of the Antarctic ice sheet, Nature Geoscience, 13, 132–137, 2020.

Nakayama, Y., Manucharyan, G., Zhang, H., Dutrieux, P., Torres, H. S., Klein, P., Seroussi, H., Schodlok, M., Rignot, E., and Menemenlis,
      D.: Pathways of ocean heat towards Pine Island and Thwaites grounding lines, Scientific reports, 9, 1–9, 2019.

655 Nye, J.: Water flow in glaciers; jökulhlaups, tunnels and veins, Journal of Glaciology., 17, 181–207, 1976.

Pattyn, F.: Antarctic subglacial conditions inferred from a hybrid ice sheet/ice stream model, Earth and Planetary Science Letters, 295,
      451–461, 2010.

Prohaska, Y.: Laboratory Experiment of Subglacial Drainage: Prototype Development, Ph.D. thesis, ETH Zurich, 2017.

Ralston, D. K., Geyer, W. R., and Lerczak, J. A.: Structure, variability, and salt flux in a strongly forced salt wedge estuary, Journal of
660   Geophysical Research: Oceans, 115, 2010.

Reese, R., Gudmundsson, G. H., Levermann, A., and Winkelmann, R.: The far reach of ice-shelf thinning in Antarctica, Nature Climate
      Change, 8, 53–57, 2018.

Robel, A. A., Seroussi, H., and Roe, G. H.: Marine ice sheet instability amplifies and skews uncertainty in projections of future sea-level rise,
      Proceedings of the National Academy of Sciences, 116, 14 887–14 892, 2019.

665 Rominger, J. T. and Nepf, H. M.: Flow adjustment and interior flow associated with a rectangular porous obstruction, Journal of Fluid
      Mechanics, 680, 636–659, 2011.

Rosevear, M. G., Gayen, B., and Galton-Fenzi, B. K.: The role of double-diffusive convection in basal melting of Antarctic ice shelves,
      Proceedings of the National Academy of Sciences, 118, 2021.

Ross, N., Bingham, R. G., Corr, H. F., Ferraccioli, F., Jordan, T. A., Le Brocq, A., Rippin, D. M., Young, D., Blankenship, D. D., and Siegert,
670   M. J.: Steep reverse bed slope at the grounding line of the Weddell Sea sector in West Antarctica, Nature Geoscience, 5, 393–396, 2012.

Rothlisberger, H.: Water pressure in intra- and subglacial channels, Journal of Glaciology., 11, 172–203, 1972.

Sayag, R. and Worster, M. G.: Elastic dynamics and tidal migration of grounding lines modify subglacial lubrication and melting, Geophysical
      Research Letters, 40, 5877–5881, 2013.

Schroeder, D. M., Blankenship, D. D., and Young, D. A.: Evidence for a water system transition beneath Thwaites Glacier, West Antarctica,
675   Proceedings of the National Academy of Sciences, 110, 12 225–12 228, 2013.

Schroeder, D. M., Grima, C., and Blankenship, D. D.: Evidence for variable grounding-zone and shear-margin basal conditions across
      Thwaites Glacier, West Antarctica, Geophysics, 81, WA35–WA43, 2016.

Seroussi, H. and Morlighem, M.: Representation of basal melting at the grounding line in ice flow models, The Cryosphere, 12, 3085–3096,
      2018.

680 Seroussi, H., Nakayama, Y., Larour, E., Menemenlis, D., Morlighem, M., Rignot, E., and Khazendar, A.: Continued retreat of Thwaites
      Glacier, West Antarctica, controlled by bed topography and ocean circulation, Geophysical Research Letters, 2017.

Seroussi, H., Nowicki, S., Simon, E., Abe-Ouchi, A., Albrecht, T., Brondex, J., Cornford, S., Dumas, C., Gillet-Chaulet, F., Goelzer, H., et al.: initMIP-Antarctica: an ice sheet model initialization experiment of ISMIP6, The Cryosphere, 13, 1441–1471, 2019.

Seroussi, H., Nowicki, S., Payne, A. J., Goelzer, H., Lipscomb, W. H., Abe Ouchi, A., Agosta, C., Albrecht, T., Asay-Davis, X., Barthel, A., Calov, R., Cullather, R., Dumas, C., Gladstone, R., Golledge, N., Gregory, J. M., Greve, R., Hatterman, T., Hoffman, M. J., Humbert, A., Huybrechts, P., Jourdain, N. C., Kleiner, T., Larour, E., Leguy, G. R., Lowry, D. P., Little, C. M., Morlighem, M., Pattyn, F., Pelle, T., Price, S. F., Quiquet, A., Reese, R., Schlegel, N.-J., Shepherd, A., Simon, E., Smith, R. S., Straneo, F., Sun, S., Trusel, L. D., Van Breedam, J., van de Wal, R. S. W., Winkelmann, R., Zhao, C., Zhang, T., and Zwinger, T.: ISMIP6 Antarctica: a multi-model ensemble of the Antarctic ice sheet evolution over the 21$^{\text{st}}$ century, The Cryosphere Discussions, 2020, 1–54, https://doi.org/10.5194/tc-2019-324, 2020.

Shepherd, A., Ivins, E., Rignot, E., Smith, B., van den Broeke, M., Velicogna, I., Whitehouse, P., Briggs, K., Joughin, I., Krinner, G., et al.: Mass balance of the Antarctic Ice Sheet from 1992 to 2017, Nature, 556, 219–222, 2018.

Shi, L., Cui, L., Park, N., and Huyakorn, P. S.: Applicability of a sharp-interface model for estimating steady-state salinity at pumping wells—validation against sand tank experiments, Journal of Contaminant Hydrology, 124, 35–42, 2011.

Strack, O.: A single-potential solution for regional interface problems in coastal aquifers, Water Resources Research, 12, 1165–1174, 1976.

Straneo, F. and Heimbach, P.: North Atlantic warming and the retreat of Greenland's outlet glaciers, Nature, 504, 36–43, 2013.

Tulaczyk, S., Mikucki, J. A., Siegfried, M. R., Priscu, J. C., Barcheck, C. G., Beem, L. H., Behar, A., Burnett, J., Christner, B. C., Fisher, A. T., et al.: WISSARD at Subglacial Lake Whillans, West Antarctica: scientific operations and initial observations, Annals of Glaciology, 55, 51–58, 2014.

Turner, J. and Veronis, G.: The influence of double-diffusive processes on the melting of ice in the Arctic Ocean: laboratory analogue experiments and their interpretation, Journal of marine systems, 45, 21–37, 2004.

van der Boog, C. G., Dijkstra, H. A., Pietrzak, J. D., and Katsman, C. A.: Double-diffusive mixing makes a small contribution to the global ocean circulation, Communications Earth & Environment, 2, 1–9, 2021.

Wåhlin, A., Graham, A., Hogan, K., Queste, B., Boehme, L., Larter, R., Pettit, E., Wellner, J., and Heywood, K.: Pathways and modification of warm water flowing beneath Thwaites Ice Shelf, West Antarctica, Science Advances, 7, eabd7254, 2021.

Walker, R. T., Parizek, B. R., Alley, R. B., Anandakrishnan, S., Riverman, K. L., and Christianson, K.: Ice-shelf tidal flexure and subglacial pressure variations, Earth and Planetary Science Letters, 361, 422–428, 2013.

Warburton, K., Hewitt, D., and Neufeld, J.: Tidal Grounding-Line Migration Modulated by Subglacial Hydrology, Geophysical Research Letters, 47, e2020GL089 088, 2020.

Werner, A. D., Bakker, M., Post, V. E., Vandenbohede, A., Lu, C., Ataie-Ashtiani, B., Simmons, C. T., and Barry, D. A.: Seawater intrusion processes, investigation and management: recent advances and future challenges, Advances in water resources, 51, 3–26, 2013.

Wilson, E. A., Wells, A. J., Hewitt, I. J., and Cenedese, C.: The dynamics of a subglacial salt wedge, Journal of Fluid Mechanics, 895, Art–No, 2020.